NEUE ENERGIEN 2020

Publizierbarer Endbericht

Programmsteuerung:

Klima- und Energiefonds

Programmabwicklung:

Österreichische Forschungsförderungsgesellschaft mbH (FFG)

Kurztitel:

ATHENS

Langtitel:

Advanced Thermoelectric Nanostructures

1 Introduction

The increasing world's demand for energy and the environmental impact of global climate change due to the combustion of fossil fuels are big challenges for the 21st century. Both, the expulsion of fossil primary energy carriers by renewable energy sources, and the efficiency increase of energy conversion processes are the most crucial engineering tasks on the way to a sustainable energy future. Thermoelectric generators provide a way to directly convert heat originating from temperature gradients into useful electrical power.

The suitability of a material to convert heat into electricity is usually quantified in terms of the figure of merit ZT. This dimensionless number is defined as

$$ZT = \frac{S^2 \sigma T}{\kappa},$$

(1)

where S is the Seebeck coefficient (or *thermoelectric power*), σ is the electronic conductivity, and T is the absolute temperature. The expression $S^2\sigma$ in the numerator is also referred to as the *power factor*. The denominator is given by $\kappa=\kappa_e+\kappa_l$, the thermal conductivity of the material, composed of the electronic contribution κ_e and the lattice contribution κ_l. The above expression clearly indicates the strategies for optimizing the thermoelectric efficiency:

- Increase Seebeck coefficient S.
- Increase electronic conductivity σ.
- Reduce thermal conductivity κ.

Today's best thermoelectric bulk materials reach ZT values around one (ZT ~ 1), a value still not high enough to enable mass market application of thermoelectric converters. These materials are typically compounds of bismuth, tellurium, lead, antimony, and silver. The dependence on rare materials such as tellurium and on partially toxic materials represents another obstacle on the way to mass markets. Over the past five decades attempts to raise ZT to values significantly above one (ZT>1) did not succeed because in bulk materials the parameters determining ZT are generally interdependent. Optimizing one physical parameter often adversely affects another. For instance, measures that increase the Seebeck coefficient often reduce the electronic conductivity, or measures that increase the electronic conductivity often increase the thermal conductivity as well. The use of thermoelectric devices has therefore been limited to small scale applications, where the benefits of thermoelectric technology outweigh the high costs.

Nanostructured thermoelectric materials are anticipated as the key technology to introduce thermoelectrics to mass markets because of their considerably improved material properties compared to the classical bulk materials. Non-toxic, widely available starting materials can be used to fabricate nanostructures with enhanced thermoelectric performance. However, these artificial nanostructures offer various additional design parameters, and thus such structures have to be carefully designed. The nature of electronic conduction, heat transport, and the influence of dimensionality, geometry, material composition, and non-idealities are all subject to investigation. The specific nanostructures considered in

this project are quantum well structures, where both electronic and heat transport take place in the in-plane direction.

A simulation software taking into account the essential physical effects is a necessary tool for the identification and optimization of designs for efficient nanostructured thermoelectric converters. This project focuses on both, the theoretical investigation of thermoelectricity in nanostructures, and the development of the simulation software for assessment of material properties and design and optimization of the nanostructures. The simulator helps understanding thermoelectric performance through investigation of material properties and device simulation, for both the electron and phonon systems of the nanostructures.

Throughout this project, calibrated simulation software for nanostructured thermoelectric devices is established. In order to meet the demand of knowledge on different physical levels, the work follows a hierarchical approach incorporating simulations on both the material level and the device level, where each simulation tool is supported by relevant experimental data.

Proper engineering of specifically patterned nanostructures will result in improved material properties and thus the ZT value in comparison with the bulk materials. A closed optimization loop is established that, incorporates several physical material aspects as well as technological application conditions. From that, valuable insights into the control of material properties and thus into the design optimization for a variety of applications can be gained. This design process will be supported by the availability of the proposed simulation software, and thus crucial time and resource savings throughout the practical development of nanostructured thermoelectric materials and devices are ensured.

Measurement data of suitable test samples as well as thermoelectric devices fabricated on production-near equipment are provided from the industrial partner O-flexx Technologies. As an important technological constraint, the focus will be put on nanostructures suitable for mass production.

Furthermore, the very limited and partially toxic starting materials currently used for thermoelectric devices can be partially replaced by nanostructures made of widely available and cheaper starting materials such as silicon and silicon-germanium alloys. Thus, up scaling and the introduction of thermoelectric technology to mass markets can be enabled with a controlled ecological and economical footprint.

The workplan of the project consists of four work packages:

1. Development of the simulation software for thermoelectric transport
2. Analysis of the electronic band structure and the electronic transport properties of 2D superlattices
3. Analysis of the phonon band structure and the thermal transport properties of 2D superlattices
4. Optimization of the superlattice such that electrical conductivity and Seebeck coefficient are enhanced, whereas the thermal conductivity is reduced.

We have analyzed the thermoelectric coefficients in one dimensional (nanowires) and two dimensional (ultra-thin layers) systems made of silicon and germanium. Atomistic electronic structure calculations and linearized Boltzmann transport theory have been employed. We were able to show that the

thermoelectric properties can be partially engineered through the electronic band structure. In this project it has been shown quantitatively how the thermoelectric properties depend on:

- Crystallographic orientation of electronic and heat transport
- Crystallographic orientation of quantum confinement
- Length scale of quantum confinement

The current view widely accepted in literature is that the thermoelectric power factor in uniform low dimensional systems will improve via an improvement in the Seebeck coefficient. However, in this project we have shown that this current view is not correct. Electrical conductivity is the quantity that dominates the thermoelectric coefficients. Therefore, it is beneficial to the power factor to engineer the electronic structure for enhanced electrical conductivity, rather than for enhanced Seebeck coefficient. We have proposed engineering strategies for performance enhancement and showed that optimal power factors can be achieved in both one dimensional and two dimensional channels fabricated in the silicon and germanium material systems.

2   Presentation of the Results

2.1 The Simulation Software Developed

The work-package involves setting up the simulation software for analyzing the thermoelectric (TE) properties of Si based nanostructures. Two sections are addressed in the simulator: i) Electronic band structure calculation, and ii) transport models.

Proper calculation of the electronic band structure is essential in the performance analysis of nanostructured devices. At the nanometer scale the electronic properties of a given structure are different from those of the bulk material. The length scale is an additional degree of freedom in design and optimization of TE properties. Channels with different confinement length scale, transport orientation and confinement orientation will have different properties. Therefore, appropriate electronic structure methods need to be applied. For this project we use mainly the atomistic tight-binding method because of its accurate calibration to experimental data, and its inherent nature and ease in handling nanostructures on the atomistic level **[Boy04, Kli07, Neo08]**.
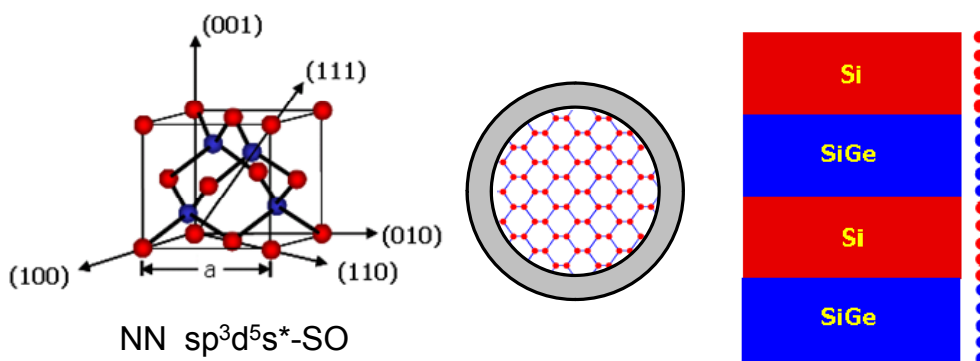

NN sp^{3}d^{5}s*-SO

Fig. 1.1: Elementary cell of the silicon lattice. Some high symmetry directions are indicated by Miller indices (left). Sketch of a cross section through a silicon nanowire grown in [110] direction (middle).Sketch of a Si/SiGe heterostructure with the number of atomic monolayers indicated on the right (right).

We have developed a simulator that computes the electronic band structure of: i) nanowires, ii) single layers, and iii) multilayers. These nanostructures are described on the atomistic level and we focus on the material system Si/SiGe. In the SiGe layers the Ge atoms are placed randomly according to the given material composition. **Figure 1.1** shows the geometry of the nanostructures considered for the simulations.
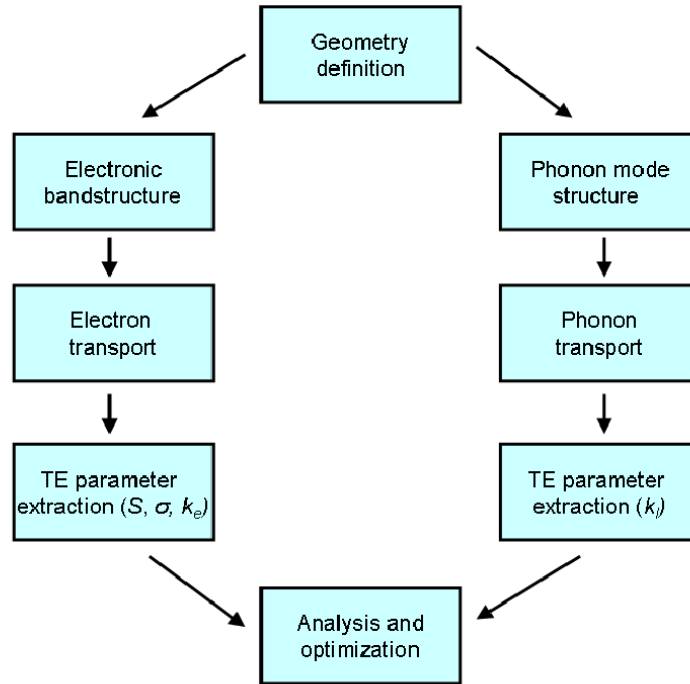
Fig. 1. 2: The modeling approach: First, the device geometry is described in close collaboration with the experimentalists who provide the dimensions and materials of the nanostructure. Left column: The electronic band structure is computed using the tight-binding scheme. That is an input to the transport simulation. After the simulations are executed, electronic conductivity σ, Seebeck coefficient S, and the electronic part of the thermal conductivity, κ_e, are extracted. The device is then be optimized to improve these parameters. Right column: Similar procedure for the lattice part of the thermal conductivity, κ_l. Finally, the device is optimized such that both constraints are met: enhancement in electrical conductivity and reduction in the thermal conductivity of the device.

The theoretical approach is summarized in **Fig. 1.2**. Here, once the geometry is defined, the electron transport (left column) and heat transport (right column) are investigated separately. The final goal is to reach a geometry optimization, which provides an enhanced ZT value. For each part, the band structure and afterwards the transport properties of electrons and phonons need to be investigated. The electronic part focuses on optimizing the power factor $S^2\sigma$, and the thermal part on the reduction of the lattice part of the thermal conductivity, κ_l (see Equation (1)).

2.2 Electronic Structure and Electronic Conductivity

In Work package 2, we calculate the electronic band structure of in nanowires and ultra-thin layers as a function of confinement length scale, confinement orientation, and transport orientation. The atomistic tight-binding model $sp^3d^5s^*$ is used.

2.2.1 Electronic structure calculation

Several typical examples of electronic structure calculations using this model are shown in **Figure 2.1**. These figures demonstrate the fact that the electronic structures depend on the length scale of quantum confinement and are strongly anisotropic. **Figures 2.1a-d** show energy landscapes for holes (i.e., the valence bands) in ultra-thin Si layers. **Figures 2.1a-b** show the electronic structure for layers with (100) surface and widths of W=15nm and W=3nm, respectively. Some anisotropy of the energy contours is observed, as well as some effect of the different widths. **Figures 2.1c-d**, show the energy contour lines for the layers with (110) surface and widths of W=15nm and W=3nm, respectively. The electronic structures resulting from the (110) and the (100) surface orientations are different. The most important observation, however, is that as the width of the (110) layer is reduced, the electronic structure dramatically changes in the [110] orientation (compare **Figures 2.1c-d)**. This will have consequences for its electronic properties as we will show below.

Figures 2.1e-f show the band structure of electrons (i.e., the conduction bands) in Si nanowires.The orientation of the nanowires is [100] and the diameters are D=3nm and D=12nm, respectively. **Figures 2.1g-h** show the band structure for electrons for Si nanowires in the [111] orientation, again for diameters D=3nm and D=12nm, respectively. What is observed here is that the electronic structure changes with orientation and diameter. **Figures 2.1k-l** show the band structure of holes (valence bands) of Si nanowires in the [100] orientation for D=3nm and D=12nm, respectively, which again show differences as the diameter is changed. **Figures 2.1m-n** show the band structure of holes in Si nanowires in the [110] orientation for D=3nm and D=12nm, respectively. Importantly, in this case, not only the number of subbands changes with diameter, but the curvature as well, which will have implications in the transport properties.
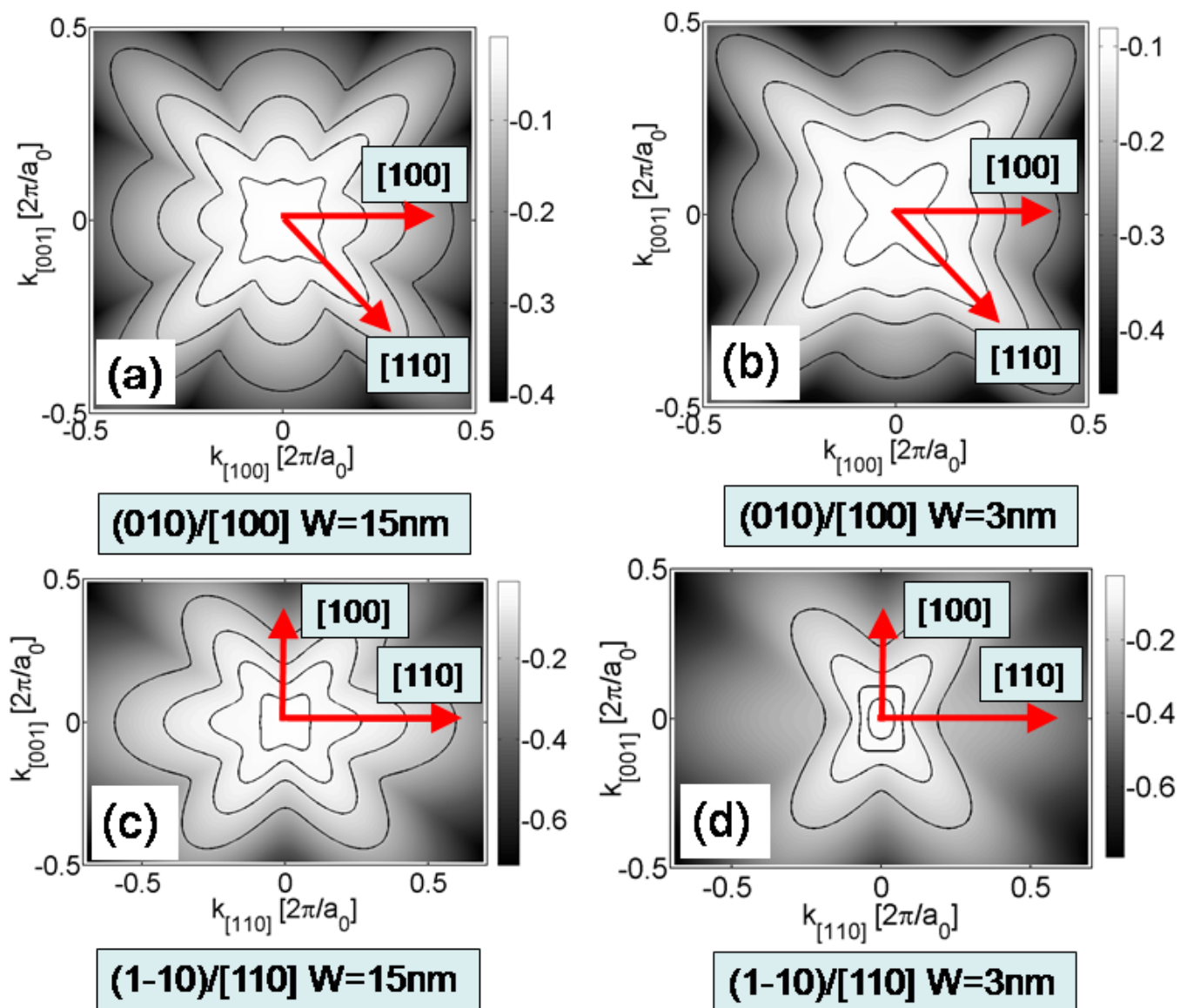
Fig. 2.1 a-d: Energy contour lines of the valence band in ultra-thin Si layers. The layer thickness is W=15nm in (a,c) and W=3nm in (b,d). The surface orientation of the layer is (100) in (a,b) and (110) in (c,d). This example demonstrates that the band structure and thus the thermoelectronic power factor (see Section 1) will depend on the surface orientation, the layer thickness, and because of the strong anisotropy also on the in-plane direction. In this parameter space the optimum parameter set has to be sought.
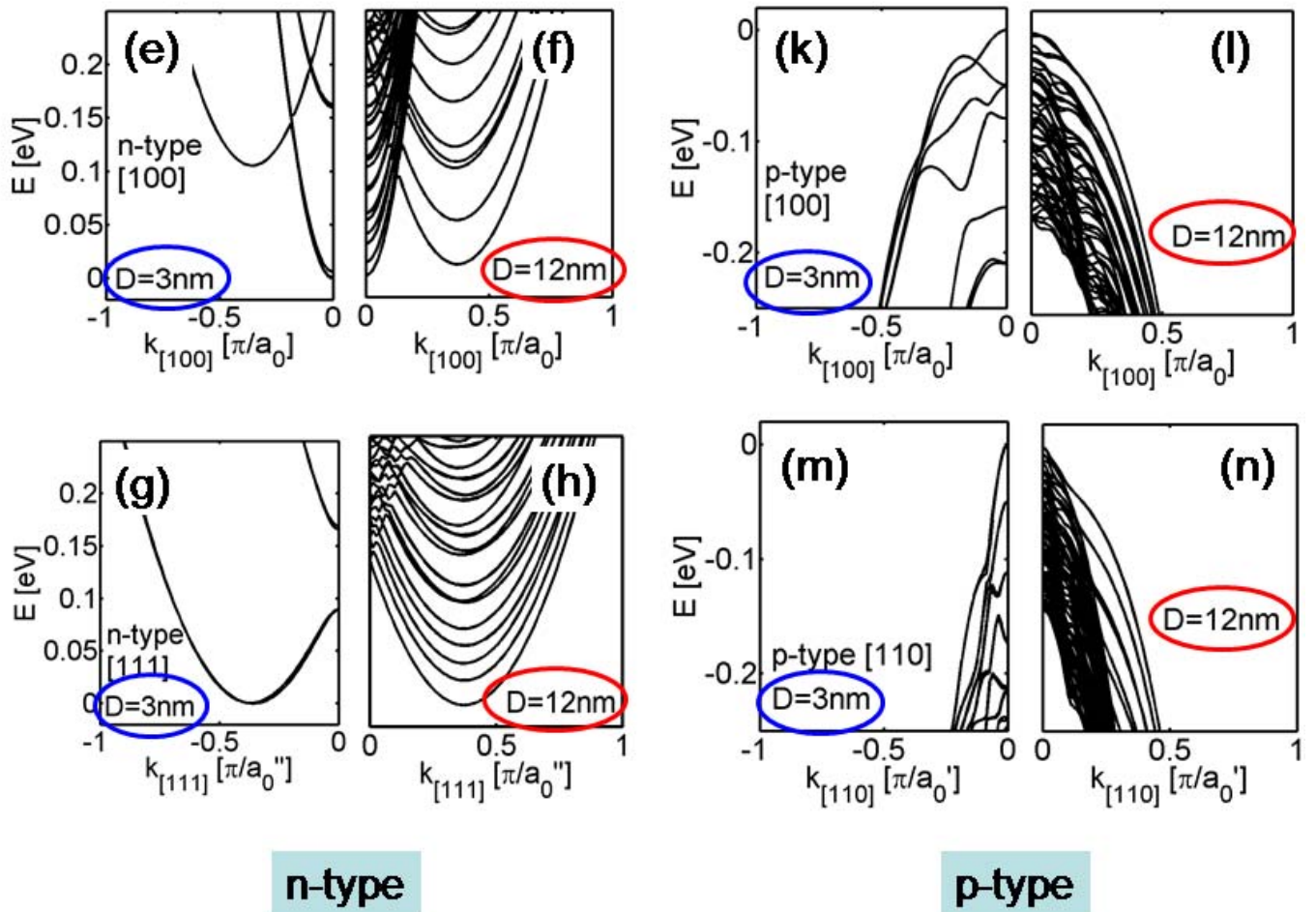
Fig. 2.1 e-n: Electronic band structures of Si nanowires. The dependence on the following parameters is shown: type of charge carrier (electrons and holes), diameter (3nm ad 12nm), and orientation of the nanowire ([100] and [111]). Again, since the band structure depends on these parameters, so does the thermoelectric power factor. An optimum parameter set has to be sought.

2.2.2 Electronic Conductivity Calculation

To calculate the electronic transport properties of the nanostructures we employ two different methods, one based on the Landauer formalism and the other on linearized Boltzmann theory.

The Landauer formalism provides an estimate of the upper limit of the thermoelectric properties. This method essentially analyses the effect of the electronic band structure alone on the thermoelectric properties, and identifies the importance of the Seebeck coefficient. It is computationally robust, and once the electronic structure is calculated, the thermoelectric coefficients of interest can be extracted within minutes of computational time. In this formalism is described in **[Kim09, Vo08].**

The approach based on linearized Boltzmann theory is computationally more costly, but provides more realistic numbers for the expected performance. For this we have included all relevant scattering processes: i) Phonons (elastic and inelastic), ii) Impurity scattering, and iii) Surface roughness scattering (SRS). The rates are calculated using the electronic dispersions and wave functions extracted from the tight-binding calculations. Details can be found in **[Mah96, Sch03]**:

II. Results

Figure 2.2 shows the extracted thermoelectric parameters for n-type [100] NWs, plotted as a function of the one-dimensional carrier concentration **[Neo10b]**. The NWs' diameters start from D=3nm (solid-black) to D=12nm (dot-black), and the blue lines indicate results for NWs with 1nm increment in diameter. The electrical conductivity of the smaller wires in **Fig. 2.2a** is shifted to the left compared to the conductivity of the larger wires. The reason is that at the same one-dimensional carrier concentration, the Fermi level is pushed at higher energies into the subbands of the narrower wires faster than in the case of the thicker NWs. In the case of the thicker wires, the Fermi level remains lower in energy (the larger number of subbands easily provides the states to be filled at the required carrier concentration). The Seebeck coefficient on the other hand, in **Fig. 2.2b**, is higher (shifted to the right) for larger diameter NWs at the same one-dimensional carrier concentration than in the narrower NW cases. The reason is that there are many more subbands which are more spread in energy. The Seebeck coefficient is proportional to the difference of the Fermi Energy form the conduction band energy, E_F-E_C, which increases as the subbands are spread in energy **[Kim09]**. The power factor σS^2, however, as shown in **Fig. 2.2c**, is favored for the smaller diameter NWs, for which the peak is almost twice as high as that of the thicker diameter ones. As the diameter decreases from D=12nm down to D=3nm the power factor is increased. For diameters larger than approx. 7nm, the peak of the power factor saturates, which indicates that in an ideal situation, performance benefits due to dimensionality will only be observed for NWs with diameters below 7nm. Similar effects are observed for the other NW family types we consider. We mention here that alternatively, one can plot σ, S and σS^2 as a function of the three-dimensional doping concentration (instead of one-dimensional). This will result in a shift of the relative positions of each curve on the x-axis depending on the NWs' area. The magnitude of the power factor peaks of wires with different diameters, however, does not change. In such case, the peaks appear less spread in the x-axis as when plotted against the one-dimensional doping values.
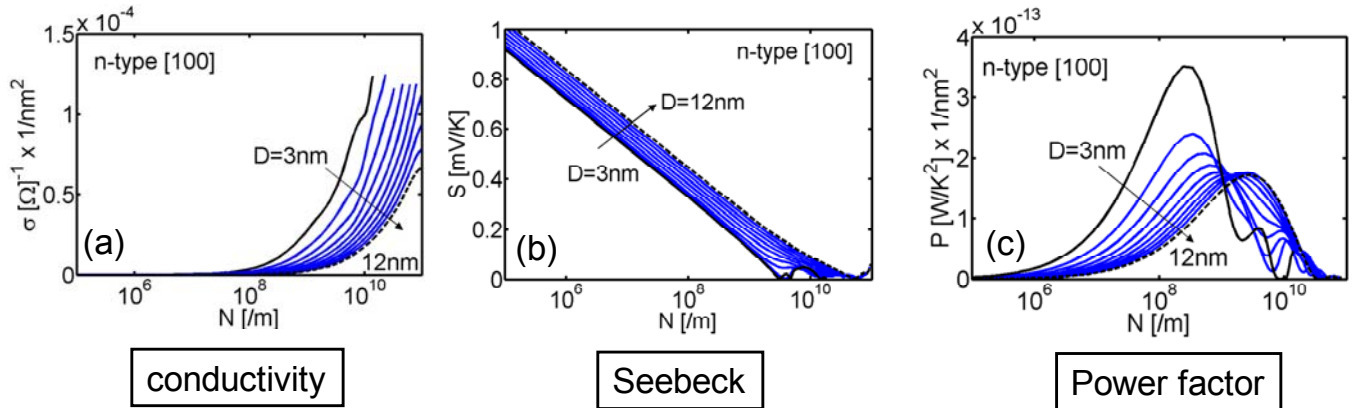
conductivity · Seebeck · Power factor

Fig. 2.2: The parameters determining the thermoelectric efficiency for n-type [100] nanowires with diameters from D=3nm (black-solid line) to D=12nm (black-dotted line) as a function of the one-dimensional doping concentration. The arrows indicate the direction of diameter increase. The results are presented with 1nm diameter increment. (a) Electronic conductivity σ. (b) Seebeck coefficient S. (c) Power factor σS^2.

The previous results considered only ballistic transport, and capture only the effect of band structure on the thermoelectric coefficients. In reality, however, as we show further down, enhanced surface roughness and phonon scattering will reduce the conductivity more drastically in NWs with smaller diameters, and the benefits described in **Fig. 2.2** may or may not be observed **[Neo11]**. To illustrate the effect of stronger phonon and SRS mechanisms for the smaller NWs, in **Fig. 8** we plot the power factor for the [100] NW for D=12nm (dashed) and D=3nm (solid). The arrow shows the direction of diameter decrease. **Figure 8a** shows the devices' power factor under *ballistic* transport conditions, extracted using the Landauer formalism **[Neo10b, Lan57, Kim09]** as in **Fig. 2.2c**, but now plotted against the 3D carrier concentration. **Figure 2.3b** shows the same result for simulations in which only phonon scattering is considered. In this case the performance of the two NWs is somewhat more similar, which means that the D=3nm NW is affected more by scattering. (Note that the units of the power factor are different in **Fig. 2.3a** and **Fig. 2.3b** since in the case of ballistic transport we compute the conductance-G instead of conductivity-σ). Finally, **Fig. 2.3c** shows results for which phonons and SRS are considered. SRS has a strong negative effect on the conductivity of the D=3nm NW, thus significantly reducing its power factor, whereas it does not affect significantly that of the D=12nm NW. We note here that the Seebeck coefficient is not affected much from case to case since it is independent of scattering at first order **[Kim09]**. The variation in performance between **Fig. 2.3a, 2.3b and 2.3c**, therefore, originates from reduction in the electrical conductivity.

Not in all cases, however, the behavior is the same. There are cases in which reduced dimensionality does not provide any advantage even in the ballistic limit. This is shown in **Fig. 2.3d** for the case of ballistic transport for p-type [110] NWs. Reducing the diameter from D=12nm to D=3nm provides little advantage to the power factor. In this case, the effective mass of the bands decreases with diameter reduction as we have shown in an earlier work **[Neo10]**. This, however, also decreases the Seebeck coefficient, and finally it provides little advantage to the power factor **[Neo10b]**. Once phonon scattering is included, however, the trends are changed. The light subbands of the smaller diameter NWs provide higher carrier velocities and phonon-limited mobilities compared to NWs with larger

diameters. The power factor is thus much higher for the *D*=3nm NW compared to the *D*=12nm one as shown in **Fig. 2.3e**. In addition, when SRS is included in the calculation in **Fig. 2.3f**, although the power factor of the *D*=3nm NW suffers more than that of the *D*=12nm, it is still superior to the *D*=12nm NW. Through careful band structure engineering, in this case, the electrical conductivity can increase significantly, and partly offset the degrading effects of SRS and enhanced phonon scattering.
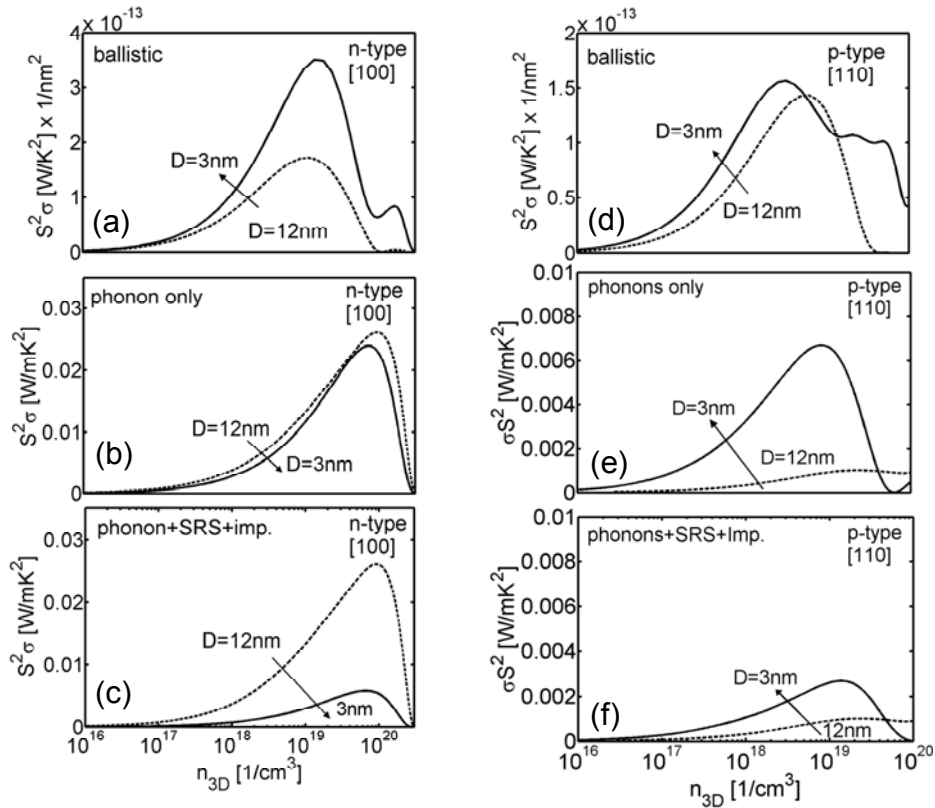

Fig. 2.3: The thermoelectric power factor for n-type NWs in [100] transport orientation for diameters *D*=3nm (solid), *D*=12nm (dash). (a) Ballistic transport conditions are considered. (b) Only phonon scattering is considered. (c) Phonon scattering, surface roughness scattering and impurity scattering are considered. (d-e-f) The same for p-type NWs in the [110] transport orientation **[Neo11]**.
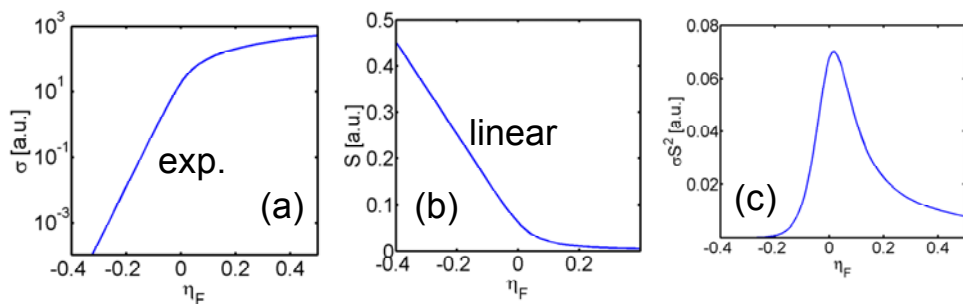

Fig. 2.4: The electrical conductivity (a) Seebeck coefficient (b) and power factor (c) versus the distance of the conduction band from the Fermi level, $\eta_F=E_C-E_F$. A simple parabolic band and scattering rates proportional to the density of final states are assumed.

Understanding the interrelation between Seebeck coefficient *S* and conductivity *σ*

Another important aspect of this work was to identify the interrelation between σ and S. In bulk materials, the two quantities are inversely proportional, as shown in **Fig. 2.4**, which keeps the power factor low, with its maximum around the band edge. At the nanoscale, however, it was suggested that this interdependence could break, and simultaneous improvement of both quantities could be achieved. Below we elaborate on the finding of this project concerning both these points.

There is a possibility to achieve improvements in S once the dimensions of the channel cross section are reduced down to a few nanometers. **Figure 2.5b** shows the Seebeck coefficient of the n-type [100] NW at carrier concentrations $n=10^{19}/cm^3$ versus the NW diameter. Indeed, an improvement in the Seebeck coefficient is observed as the diameter is reduced below 6-7nm. This is a clear indication that any benefits due to the low-dimensionality on the power factor in Si based structures will appear for length scales below 6-7nm. This seems to be insensitive to the scattering mechanisms that take place during transport in the NW. The Seebeck coefficient increase, however, is only moderate, of the order of 70% as the diameter is scaled to D=3nm. This increase originates almost exclusively from the increase in the reduced Fermi level $\eta_F=E_C-E_F$ as the diameter is reduced. The Seebeck coefficient has a linear dependence on η_F as it shown in **Fig. 2.4b**.
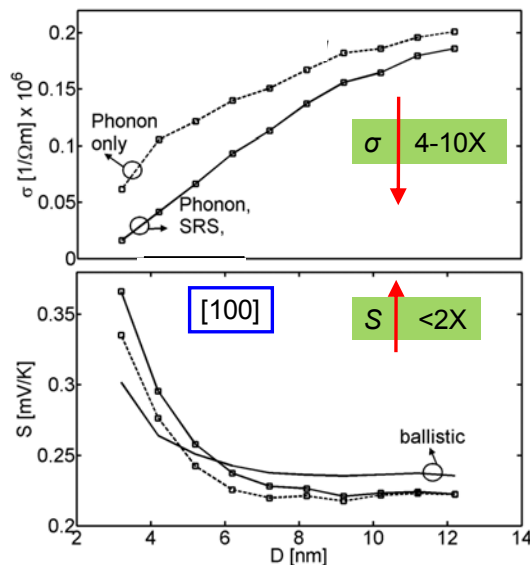

Fig. 2.5: (a) The electrical conductivity of the n-type [100] NW versus diameter. Cases for phonon limited (dashed-squared), and phonon- plus surface roughness-limited conductivity (solid-squared) are shown. (b) The Seebeck coefficient. Cases for ballistic transport (solid), phonon limited (dashed-squared), and phonon- plus surface roughness-limited (solid-squared) are shown.

Although improvements in the Seebeck coefficient could be achieved, a main conclusion of this work is that in contrast to common view, these improvements lead to a much larger inevitable degradation in the electrical conductivity. Power factor improvements cannot, therefore, be achieved through Seebeck improvements. The conductivity is an exponential function of η_F, whereas S is a linear

function of η_F. Therefore, changes in η_F resulting from different electronic structures in various low dimensional channels will affect the conductivity exponentially, but affect the Seebeck coefficient only linearly, (and in an inverse way). The conductivity, therefore, is affected much more than the Seebeck coefficient. This is observed in **Fig. 2.5a**, which shows the conductivity as a function of diameter. The phonon-limited conductivity drops by almost 4X as the diameter is reduced. In reality, it could drop by ~10X once surface roughness scattering is considered. This results in power factor degradation with diameter.

2.3 Phonon Band Structure and Thermal Conductivity

A proper calculation of the vibrational modes of the crystal lattice is very important in the performance analysis of nanostructured devices. To investigate the thermal properties of silicon-based nanostructures, we need to appropriately describe the dynamics of atoms and the inter-atomic potential energy. One of the most popular models used for zinc-blend and diamond structures is valence force field (VFF) model, also known as the Keeting model. This model, however, is not to be accurate enough in the entire Brillouin zone, even for bulk silicon. By adding three other terms to the Keating VFF model **[Kea66]**, cross bond stretching, cross bending stretching, and coplanar bond bending interactions, the model can capture the details of phononic band structures in the entire bulk Brillouin zone. This extended model is referred to as the Modified VFF (MVFF) model **[Sui93, Pau10]**. We have implemented this model in order study the phonon properties of nanostructures on an atomistic level. The results obtained from this model include the sound velocity, the heat capacity, and the lattice part of the thermal conductivity.

Figure 3.1a shows the longitudinal (solid) and transverse (dashed) sound velocities of the [100], [110], and [111] NWs as a function of the NW side length. There are two important observation is this figure. First, the velocities are very anisotropic, and second, they tend to decrease as the confinement length scale is reduced below 3nm. The specific heat on the other hand is very similar for all NWs, and increases as the cross section of the NW is reduced (**Fig. 3.1b**). Finally, our results indicate that the thermal conductivity is anisotropic as shown in **Fig. 3.1c**, with the [110] NW having the largest thermal conductance, followed by the [100] NW, whereas the [111] NW has the lowest thermal conductance. The reduction in thermal conductance with decreasing diameter can be exploited to enhance thermoelectric efficiency, as indicated by equation (1).
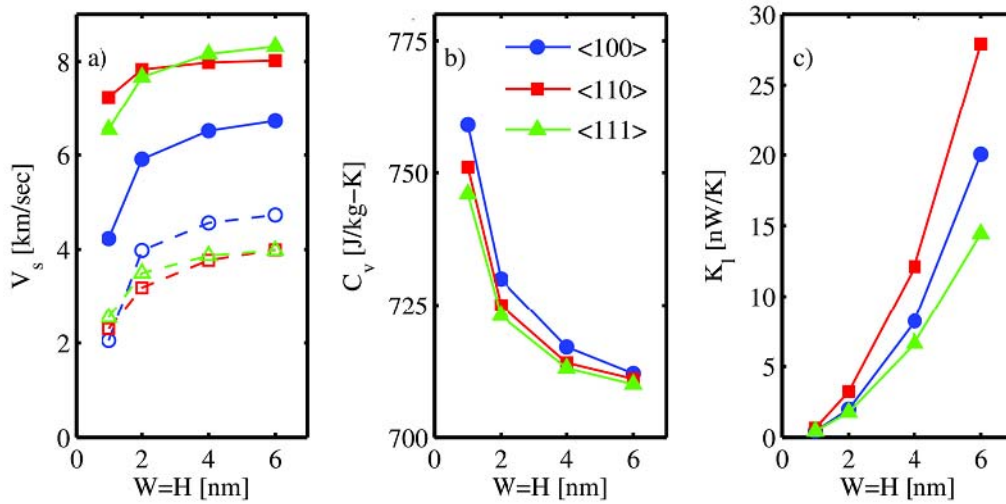
Fig. 3.1: (a) Sound velocity, (b) specific heat, and (c) ballistic thermal conductance as a function of the diameter of square silicon nanowires. Three different nanowire orientations are considered. Longitudinal and transverse sound velocities are shown with solid and dashed lines, respectively.

3 Conclusions

In this project, we investigated the thermoelectric properties of silicon nanowires and ultra-thin silicon layers. A simulation program based on accurate physical models has been developed and used for this theoretical investigation.

This investigation clearly shows that the thermoelectric properties of these nanostructures can to some extent be tailored by band structure engineering. The band structure and therefore the thermoelectric properties depend on the following parameters: growth direction and diameter of the nanowire; and, in the case of ultra-thin layers, on the growth direction, the layer thickness (width) and the in-plane direction of thermoelectric transport. Parameter sets that enhance the thermoelectric properties of the considered nanostructures have been identified.

Our theoretical findings indicate that the electrical conductivity is the quantity that dominates the thermoelectric coefficients. For the given material, one should aim at improving the conductivity by nanostructuring or other measures, rather than improving the Seebeck coefficient. We demonstrated that the sharp edges in the density of states, that in the literature are widely believed to improve the Seebeck coefficient, actually do not provide the expected result. It is beneficial to the thermoelectric power factor, therefore, to engineer the electronic band structure for enhanced electrical conductivity, rather than for enhanced Seebeck coefficient. This is an important guideline for the future development of highly efficient nanostructured thermoelectrics.

In a thermoelectric converter usually two materials are connected, one with positive and one with negative Seebeck coefficient. Therefore, both p-type and n-type semiconducting nanostructures with enhanced thermoelectric properties are required. This study shows that band structure engineering is

very beneficial in particular for the p-type nanostructures. Enhanced ZT values up to four times have been predicated once the materials are properly optimized. The optimum parameter ranges for the p-type nanostructures, as identified in this project, are summarized in the following:

- For **p-type silicon nanowires**, the [111] orientation is clearly the optimum. At diameters below 4nm the quantization effect gives an additional enhancement of the ZT value.

- For **p-type silicon thin films**, the (110) surface orientation combined with the [110] transport direction is found to be the optimum. Below 6nm film thickness, an additional enhancement of ZT due to quantization is observed.

The optimal doping concentrations were found to be in the range from $1 \cdot 10^{19}$ to $2 \cdot 10^{19}$ cm^{-3}.

For the n-type nanostructures, on the other hand, the gain from band structure engineering is not so pronounced. Enhancements of ZT in the range of only 10 to 20% have been observed. In the case of n-type nanowires, at diameters above 10nm the [100] orientation is beneficial, and otherwise the [111] orientation. In all cases, however, n-type and p-type, proper optimization can provide ZT values of unity or larger, which sets the stage for Si based channels as efficient thermoelectric materials, and makes it comparable to the best to date thermoelectric materials.

4   Outlook

The study performed in this project represents a first step towards the development of mass-producible, highly efficient thermoelectric converters, fabricated from widely available and non-toxic materials. Nanostructuring is employed to enhance the ZT value of the material and thus the efficiency of the thermoelectric converter. The thermoelectric properties of ultra-narrow silicon nanowires and ultra-thin silicon layers have been studied. Multilayer systems can be fabricated using planar technology, so that the most advanced manufacturing concepts from the semiconductor, photovoltaic and MEMS industries can be used.

While this study focused solely on the development of high ZT materials, on the way to a final product additional steps have to be taken. Contact technology especially at the hot end of the converter, reliability under thermal cycles, packaging of the thermoelectric modules, low-loss connection to the thermal heat bath are additional issues to be addressed. Once ZT values above three can be achieved (ZT > 3), energy harvesting by thermoelectric converters is commonly believed to become an economically viable technology for energy production.

5   Literature

5.1 Journal publications produced from this work

[Neo10] N. Neophytou, S. G. Kim, G. Klimeck, and H. Kosina, J. Appl. Phys., 107, 113701, 2010.

[Neo10b] N. Neophytou, M. Wagner, H. Kosina, and S. Selberherr, J. Electr. Mater.,vol 39, no. 9, pp. 1902-1908, 2010.

[NeoNL10] N. Neophytou and H. Kosina, Nano Lett., vol. 10, no. 12, pp. 4913-4919, 2010.

[Neo11] N. Neophytou and H. Kosina, J. Electr. Mater., vol. 40, no. 5, pp. 753-758, 2011.

[NeoJAP11] N. Neophytou, G. Klimeck, and H. Kosina, J. Appl. Phys., vol. 109, p. 053721, 2011.

[NeoPRB11a] N. Neophytou and H. Kosina, Physical Review B, 84, 085313, 2011.

[NeoPRB11b] N. Neophytou and H. Kosina, Physical Review B, Vol. 83, 245305, 2011.

[NeoAPL11] N. Neophytou and H. Kosina, Applied Physics Letters, 99, 092110, 2011.

[NeoSSE12] N. Neophytou and H. Kosina, Solid State Electronics, 2012.

[KarJAP12] H. Karamitaheri, N. Neophytou, M. Pourfath, R. Faez, and H. Kosina, J. Appl. Phys. 111, 054501, 2012.

[NeoJCE12] N. Neophytou and H. Kosina, Journal of Computational Electronics, 2012, DOI: 10.1007/s10825-012-0383-1 (invited).

[NeoJEM12] N. Neophytou and H. Kosina, Journal of Electronic Materials, DOI: 10.1007/s11664-011-1891-7, 2012.

[KarJCE12] H. Karamitaheri, N. Neophytou, M. Pourfath, and H. Kosina, Journal of Computational Electronics, DOI: 10.1007/s10825-011-0380-9, 2011, (invited).

[NeoEDL12] N. Neophytou and H. Kosina, IEEE EDL, in print, 2012.

5.2 Presentations of the current work in scientific conferences

[1] N. Neophytou and H. Kosina, "Thermoelectric Properties of Low-Dimensional Si and Ge Based Nanostructures", American Physical Society (APS), March Meeting, Boston, MA, USA, 2012.

[2] N. Neophytou and Hans Kosina, "Gate Field Induced Bandstructure and Mobility Variations in p-type Silicon Nanowires" Workshop on Silicon on Insulator Technology, Devices and Circuits, EUROSOI 2012, Montpellier, France, January 2012.

[3] H. Karamitaheri, M. Pourfath, N. Neophytou, M. Pazoki, and H. Kosina, "First principle study of ballistic thermal conductance of grapheneantidot lattices for thermoelectric applications," Workshop on Carbon-based low-dimensional Materials, CARBOMAT 2011, Catania, Italy.

[4] N. Neophytou and H. Kosina, "Thermoelectric Power Factor of Low Dimensional Silicon Nanostructures", European Conference on Thermoelectrics, ECT, Thessaloniki, Greece, September 2011.

[5] N. Neophytou and H. Kosina, "Strong Anisotropy and Diameter Effects on the Low-Field Mobility of Silicon Nanowires", IEEE SISPAD, Osaka, Japan, Sept. 8 – 10, 2011.

[6] N. Neophytou and H. Kosina, "Thermoelectric Power Factor of Narrow Silicon Nanowires from Atomistic Considerations", International Conference on Thermoelectrics, ICT, Traverse City, Michigan, USA, July, 2011.

[7] N. Neophytou and H. Kosina, "Atomistic simulations of electronic and thermoelectric transport in Si nanowires: Influence of confinement and orientation", Nanowires 2011, NW11, Plomari, Lesvos, Greece, June 2011.

[8] N. Neophytou and Hans Kosina, "Thermoelectric Properties of Ultra Narrow Silicon Nanowires from Atomistic Calculations", American Physical Society (APS), March Meeting, Dallas, TX, USA, 2011.

[9] N. Neophytou and H. Kosina, "Confinement Induced Mobility Increase in p-type [110] and [111] Silicon Nanowires", Workshop on Silicon on Insulator Technology, Devices and Circuits, EUROSOI 2011, Granada, Spain, January 2011.

[10] N. Neophytou, G. Klimeck, and H. Kosina, "A comprehensive atomistic analysis of bandstructure velocities in Si nanowires", International Workshop on Computational Electronics, IWCE-14, Pisa, Italy, October 2010.

[11] N. Neophytou, M. Wagner, and H. Kosina, "Atomistic analysis of thermoelectric properties of silicon nanowires", European Conference on Thermoelectrics, ECT, Como, Italy, September 2010.

[12] N. Neophytou and H. Kosina, "Thermoelectric Properties of Scaled Silicon Nanowires Using the sp3d5s*-SO Atomistic Tight-Binding Model and Boltzmann Transport", International Conference on Thermoelectrics, ICT, Shanghai, China, May-June, 2010.

[13] N. Neophytou and H. Kosina, "Atomistic Analysis of Thermoelectric Properties of Ultra Narrow Nanowires", American Physical Society (APS), March Meeting, Portland, OR, USA, 2010.

5.3 References

[Boy04] T. B. Boykin, G. Klimeck, and F. Oyafuso, Phys. Rev. B, vol. 69, pp. 115201-115210, 2004.

[Kli07] G. Klimeck, S. Ahmed, H. Bae, N. Kharche, S. Clark, B. Haley, S. Lee, M. Naumov, H. Ryu, F. Saied, M. Prada, M. Korkusinski, and T. B. Boykin, IEEE Trans. Electr. Dev., vol. 54, no. 9, pp. 2079-2089, 2007.

[Neo08] N. Neophytou, A. Paul, M. Lundstrom, and G. Klimeck, IEEE Trans. Elect. Dev., vol. 55, no. 6, pp. 1286-1297, 2008.

[Kim09] R. Kim, S. Datta, and M. S. Lundstrom, J. Appl. Phys., vol. 105, p. 034506, 2009.

[Vo08] T. T.M. Vo, A. J. Williamson, and V. Lordi, Nano Lett., vol. 8, no. 4, pp. 1111-1114, 2008.

[Mah96] G. D. Mahan and J. O. Sofo, Proc. Natl. Acad. Sci. USA, vol. 93, pp. 7436-7439, 1996.

[Sch03] T. J. Scheidemantel, C. A.-Draxl, T. Thonhauser, J. V. Badding, and J. O. Sofo, Phys. Rev. B, vol. 68, p. 125210, 2003.

[Lan57] R. Landauer, IBM J. Res. Dev., vol. 1, p. 223, 1957.

[Kea66] P. N. Keating, Phys. Rev. 145, 637, 1966.

[Sui93] Z. Sui and I. P. Herman, Phys. Rev. B, vol. 48, 17938, 1993.

[Paul10] A. Paul, M. Luisier, and G. Klimeck, J. Comput. Electron.9, 160, 2010.

[NeoTNT08] N. Neophytou, A. Paul, and G. Klimeck, IEEE Trans. Nanotechnol., vol. 7, no. 6, pp. 710-719, 2008.

6   Glossary

MVFF	Modified Valence Force Field
NN	Nearest-Neighbor
NW	Nanowire
SL	Superlattice
SRS	Surface Roughness Scattering
TB	Tight-Binding
TE	Thermoelectric
S	Seebeck coefficient
SO	Spin-Orbit
VFF	Valence Force Field